

Supporting Information for:

Insights into Cisplatin Binding to Uracil and Thiouracils from IRMPD Spectroscopy and Tandem Mass Spectrometry

Davide Corinti¹, Maria Elisa Crestoni^{*1}, Barbara Chiavarino¹, Simonetta Fornarini¹, Debora Scuderi,² and Jean-Yves Salpin^{*3,4}

1) Dipartimento di Chimica e Tecnologie del Farmaco, Università di Roma “La Sapienza”, P.le A. Moro 5, 00185 Roma, ITALY

2) Université Paris-Saclay, CNRS, Institut de Chimie Physique UMR8000, 91405, Orsay, France

3) Université Paris-Saclay, CNRS, Univ Evry, LAMBE, Evry-Courcouronnes, 91025, France

4) CY Cergy Paris Université, LAMBE, Evry-Courcouronnes, 91025, France

Corresponding Authors:

mariaelisa.crestoni@uniroma1.it (M.E.C.)

jeanyves.salpin@univ-evry.fr (J.-Y.S.)

Contents:

Computational Details. Any additional computational detail and material (xyz files of computed structures, calculated vibrational frequencies for all structures, etc.) is available from the authors upon request.

Figure S1. CID mass spectrum recorded upon activation of the *cis*-[PtCl(NH₃)₂(2SU)]⁺ ion (*m/z* 391) using a collision energy of 5 eV.

Figure S2. CID mass spectrum recorded upon activation of the *cis*-[PtCl(NH₃)₂(4SU)]⁺ ion (*m/z* 391) using a collision energy of 5 eV.

Figure S3. CID mass spectrum recorded upon activation of the *cis*-[PtCl(NH₃)₂(24SU)]⁺ ion (*m/z* 407) using a collision energy of 5 eV.

Figure S4. Breakdown curves for *cis*-[PtCl(NH₃)₂(2SU)]⁺. The red profile reports the precursor ion decay, while the blue profile shows the increasing abundance of the sum of all the product ions. The retarding potential experiment performed to obtain the corrected ECM is presented in the bottom panel.

Figure S5. Breakdown curves for *cis*-[PtCl(NH₃)₂(4SU)]⁺. The red profile reports the precursor ion decay, while the blue profile shows the increasing abundance of the sum of all the product ions. The retarding potential experiment performed to obtain the corrected ECM is presented in the bottom panel.

Figure S6. Breakdown curves for *cis*-[PtCl(NH₃)₂(24SU)]⁺. The red profile reports the precursor ion decay, while the blue profile shows the increasing abundance of the sum of all the product ions. The retarding potential experiment performed to obtain the corrected ECM is presented in the bottom panel.

Figure S7. Positive ESI mass spectra recorded upon selection of *cis*-[PtCl(NH₃)₂(U)]⁺ ion (*m/z* 375-379), in a hybrid FT-ICR tandem mass spectrometer (APEX-Qe Bruker Daltonics) after irradiation with CLIO FEL light on resonance at 1800 cm⁻¹.

Figure S8. Positive ESI mass spectra recorded upon selection of *cis*-[PtCl(NH₃)₂(2SU)]⁺ ion (*m/z* 391-395), in a hybrid FT-ICR tandem mass spectrometer (APEX-Qe Bruker Daltonics) after irradiation with CLIO FEL light on resonance at 1488 cm⁻¹.

Figure S9. Positive ESI mass spectra recorded upon selection of *cis*-[PtCl(NH₃)₂(4SU)]⁺ ion (*m/z* 391-395), in a hybrid FT-ICR tandem mass spectrometer (APEX-Qe Bruker Daltonics) after irradiation with CLIO FEL light on resonance at 1280 cm⁻¹.

Figure S10. Positive ESI mass spectra recorded upon selection of *cis*-[PtCl(NH₃)₂(24dSU)]⁺ ion (*m/z* 407-411), in a hybrid FT-ICR tandem mass spectrometer (APEX-Qe Bruker Daltonics) after irradiation with CLIO FEL light on resonance at 1285 cm⁻¹.

Figure S11. Optimized geometries and relative free energy values (at the B3LYP/LACV3P/6-311G** level) at 298 K (kJ mol⁻¹) of *cis*-[PtCl(NH₃)₂(U)]⁺. Noncovalent interactions are marked by dashed lines. Distances are given in Å.

Figure S12. Optimized geometries and relative free energy values (at the B3LYP/LACV3P/6-311G** level) at 298 K (kJ mol⁻¹) of *cis*-[PtCl(NH₃)₂(2SU)]⁺. Noncovalent interactions are marked by dashed lines. Distances are given in Å.

Figure S13. Optimized geometries and relative free energy values (at the B3LYP/LACV3P/6-311G** level) at 298 K (kJ mol⁻¹) of *cis*-[PtCl(NH₃)₂(4SU)]⁺. Noncovalent interactions are marked by dashed lines. Distances are given in Å.

Figure S14. Optimized geometries and relative free energy values (at the B3LYP/LACV3P/6-311G** level) at 298 K (kJ mol⁻¹) of *cis*-[PtCl(NH₃)₂(24dSU)]⁺. Noncovalent interactions are marked by dashed lines. Distances are given in Å.

Table S1. Thermodynamic data for the lowest energy conformers and isomers of *cis*-[PtCl(NH₃)₂(U)]⁺ calculated at the B3LYP/LACV3P/6-311G** level of theory.

Table S2. Thermodynamic data for the lowest energy conformers and isomers of *cis*-[PtCl(NH₃)₂(L)]⁺ (L=2SU, 4SU, 24dSU) calculated at the B3LYP/LACV3P/6-311G** level of theory.

Table S3. Experimental and computed IR vibrational bands for *cis*-[PtCl(NH₃)₂(U)]⁺.

Table S4. Experimental and computed IR vibrational bands for *cis*-[PtCl(NH₃)₂(2SU)]⁺.

Table S5. Experimental and computed IR vibrational bands for *cis*-[PtCl(NH₃)₂(4SU)]⁺.

Table S6. Experimental and computed IR vibrational bands for *cis*-[PtCl(NH₃)₂(24dSU)]⁺.

Reference for Gaussian 09

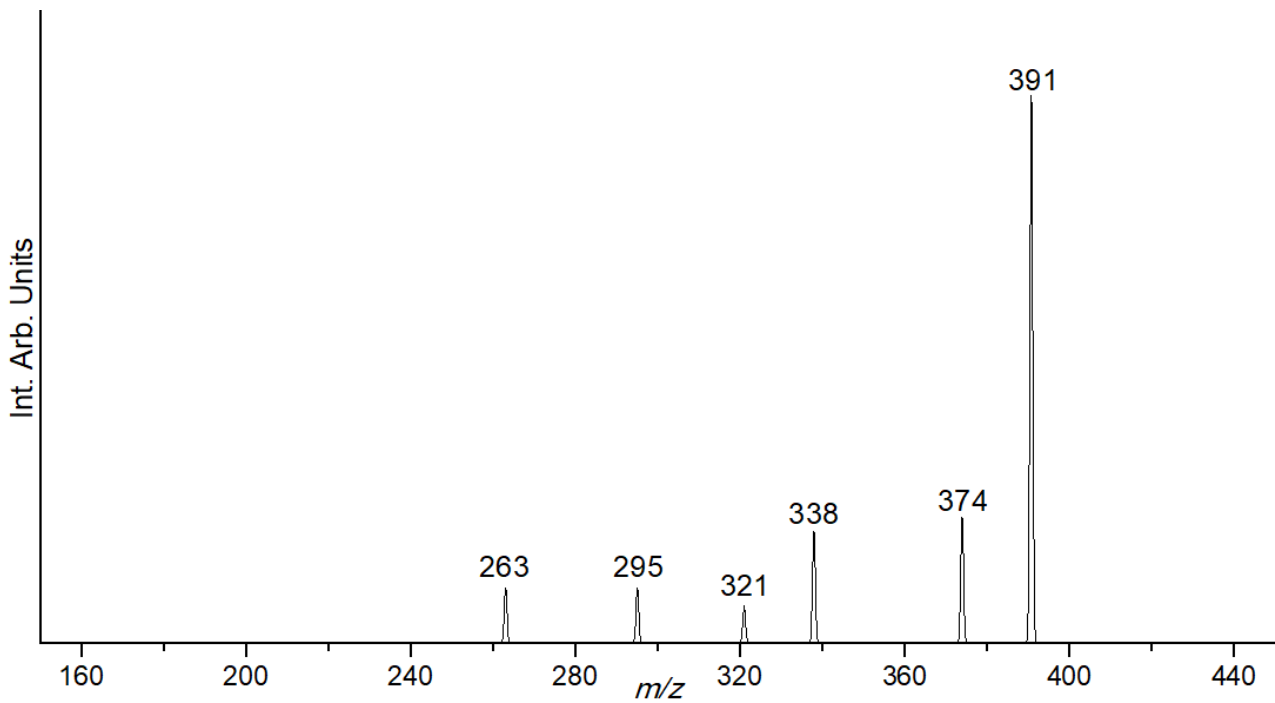


Figure S1. CID mass spectrum recorded upon activation of the cis - $[\text{PtCl}(\text{NH}_3)_2(2\text{SU})]^+$ ion (m/z 391) using a collision energy of 5 eV.

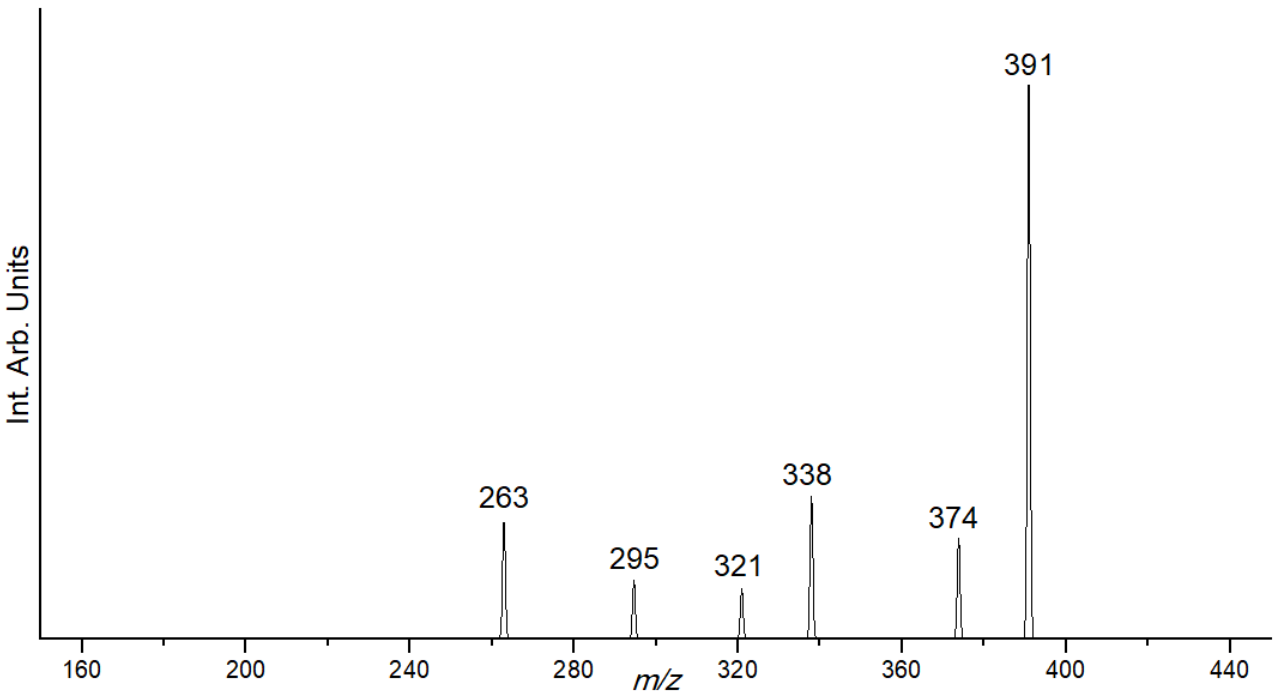


Figure S2. CID mass spectrum recorded upon activation of the cis - $[\text{PtCl}(\text{NH}_3)_2(4\text{SU})]^+$ ion (m/z 391) using a collision energy of 5 eV.

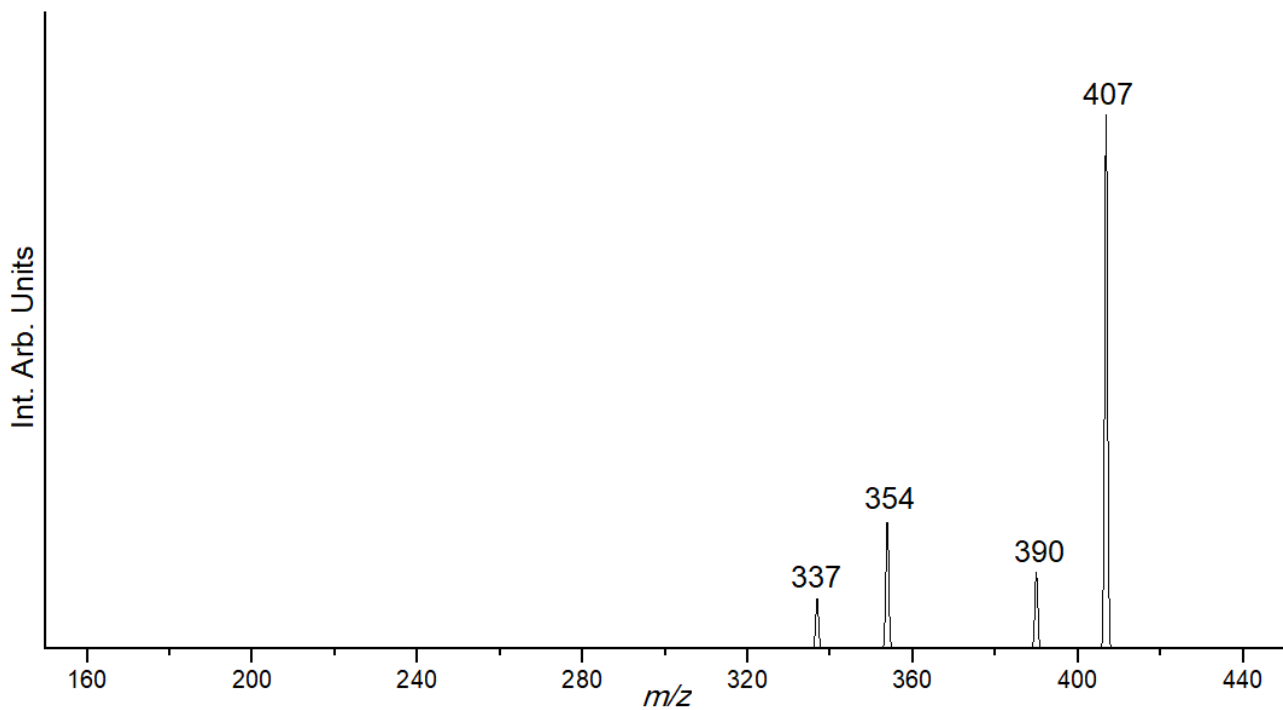


Figure S3. CID mass spectrum recorded upon activation of the *cis*-[PtCl(NH₃)₂(24SU)]⁺ ion (m/z 407) using a collision energy of 5 eV.

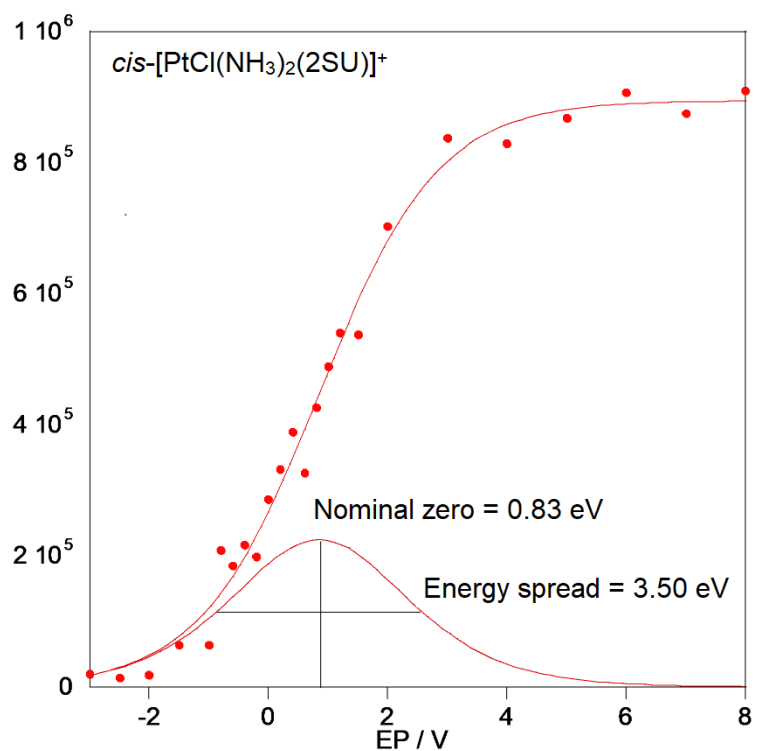
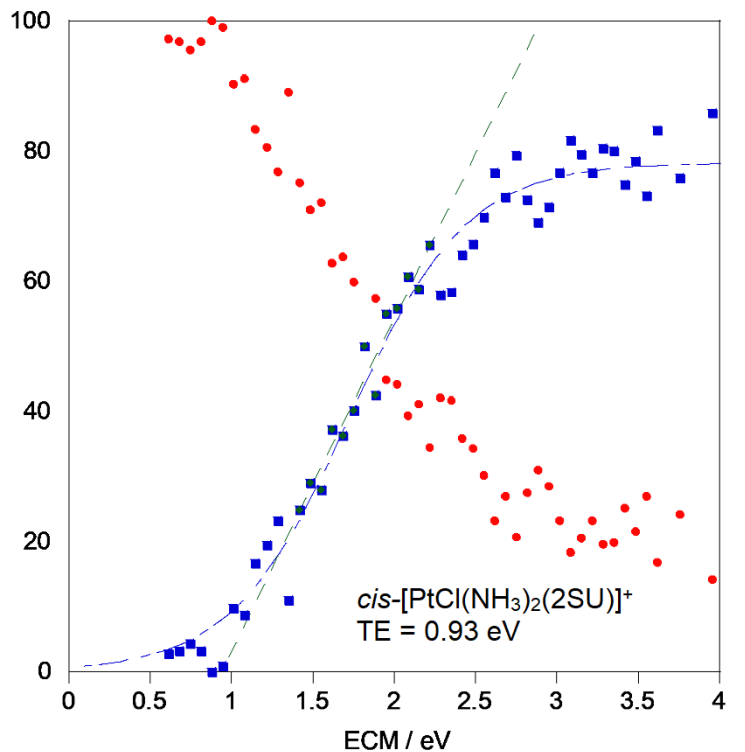


Figure S4. Breakdown curves for *cis*-[PtCl(NH₃)₂(2SU)]⁺. The red profile reports the precursor ion decay, while the blue profile shows the increasing abundance of the sum of all the product ions. The retarding potential experiment performed to obtain the corrected ECM is presented in the bottom panel.

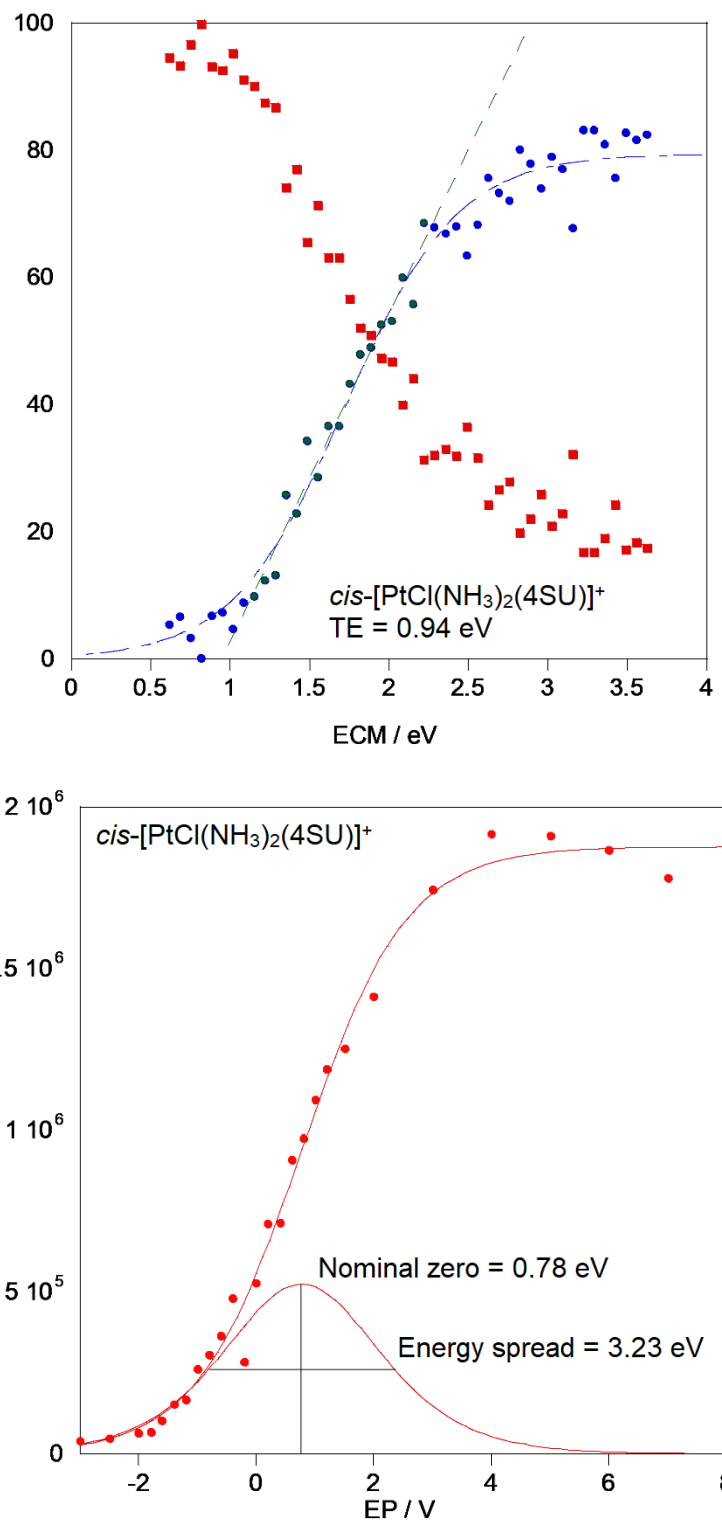


Figure S5. Breakdown curves for *cis*-[PtCl(NH₃)₂(4SU)]⁺. The red profile reports the precursor ion decay, while the blue profile shows the increasing abundance of the sum of all the product ions. The retarding potential experiment performed to obtain the corrected ECM is presented in the bottom panel.

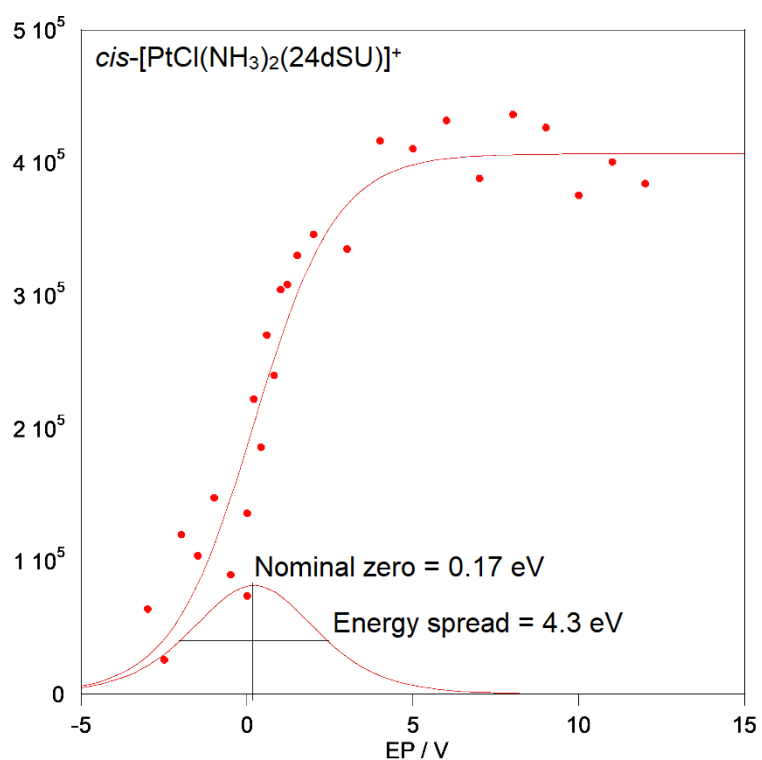
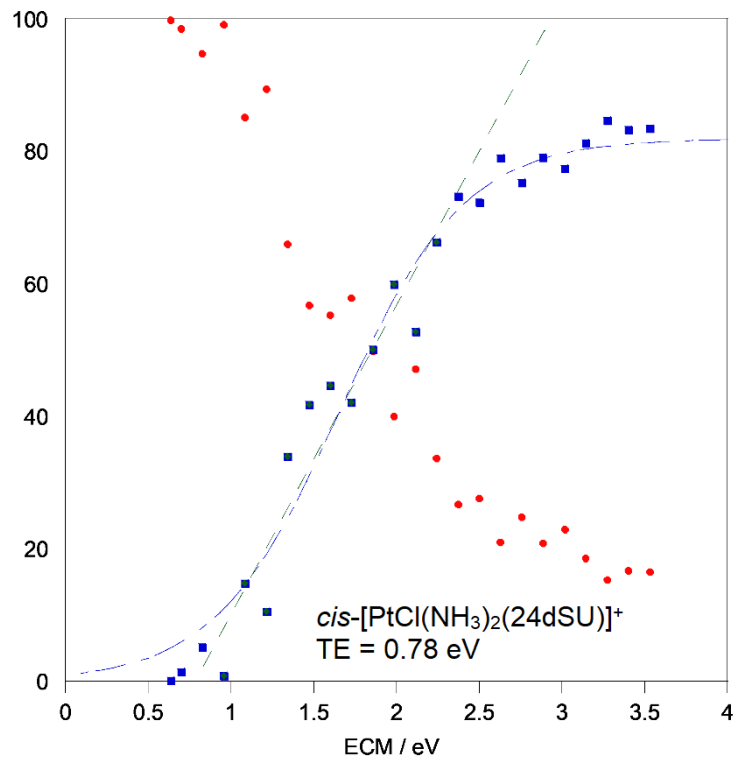


Figure S6. Breakdown curves for $cis\text{-}[PtCl(NH_3)_2(24dSU)]^+$. The red profile reports the precursor ion decay, while the blue profile shows the increasing abundance of the sum of all the product ions. The retarding potential experiment performed to obtain the corrected E_{CM} is presented in the bottom panel.

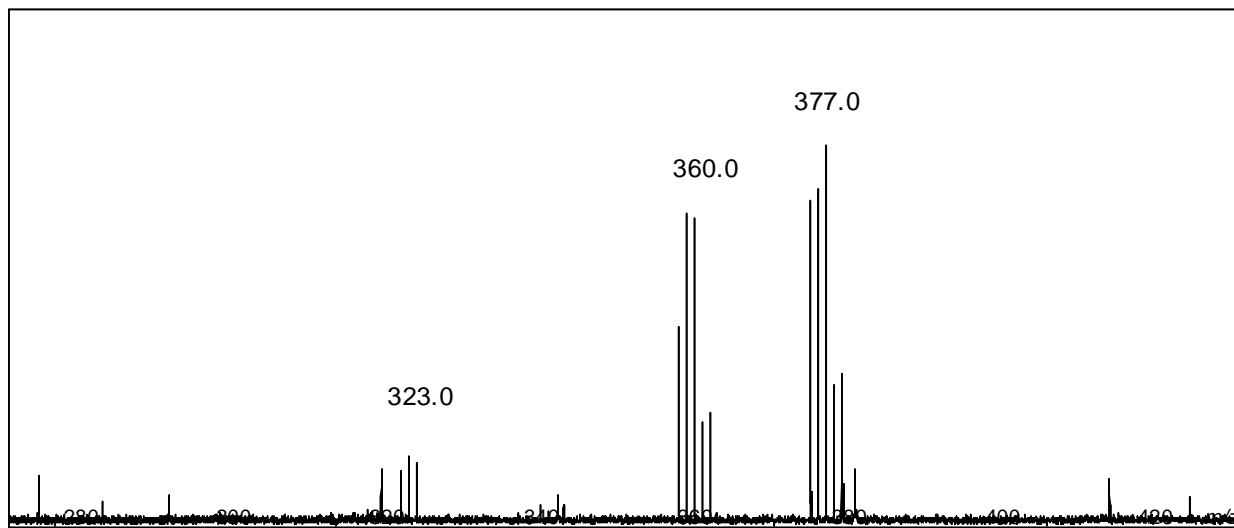


Figure S7. Positive ESI mass spectrum recorded upon selection of *cis*-[PtCl(NH₃)₂(U)]⁺ ion (m/z 375-379), in a hybrid FT-ICR tandem mass spectrometer (APEX-Qe Bruker Daltonics) after irradiation with CLIO FEL light on resonance at 1800 cm⁻¹.

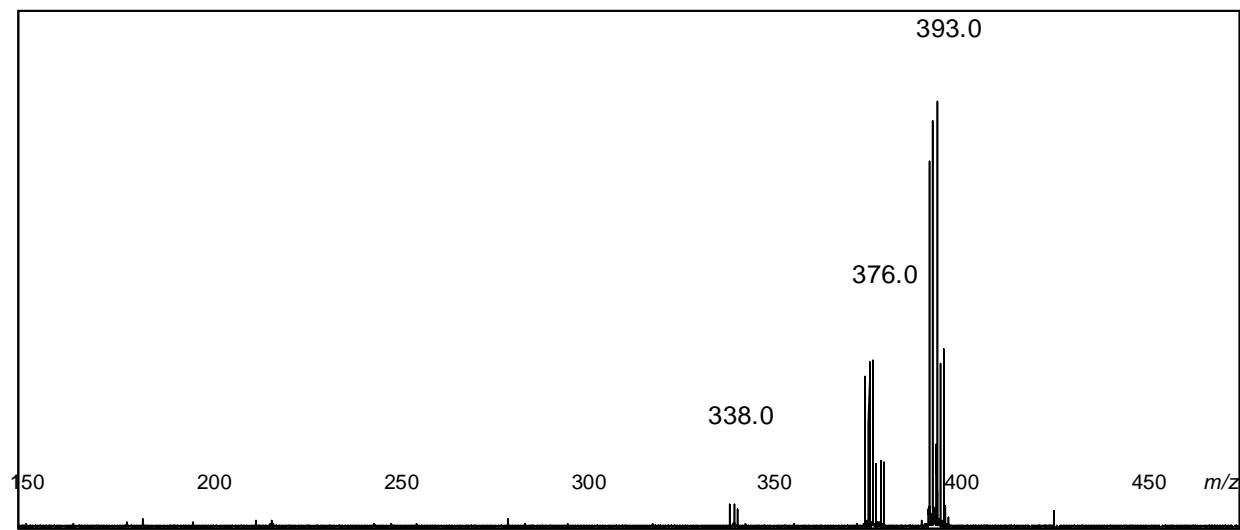


Figure S8. Positive ESI mass spectrum recorded upon selection of *cis*-[PtCl(NH₃)₂(2SU)]⁺ ion (m/z 391-395), in a hybrid FT-ICR tandem mass spectrometer (APEX-Qe Bruker Daltonics) after irradiation with CLIO FEL light on resonance at 1488 cm⁻¹.

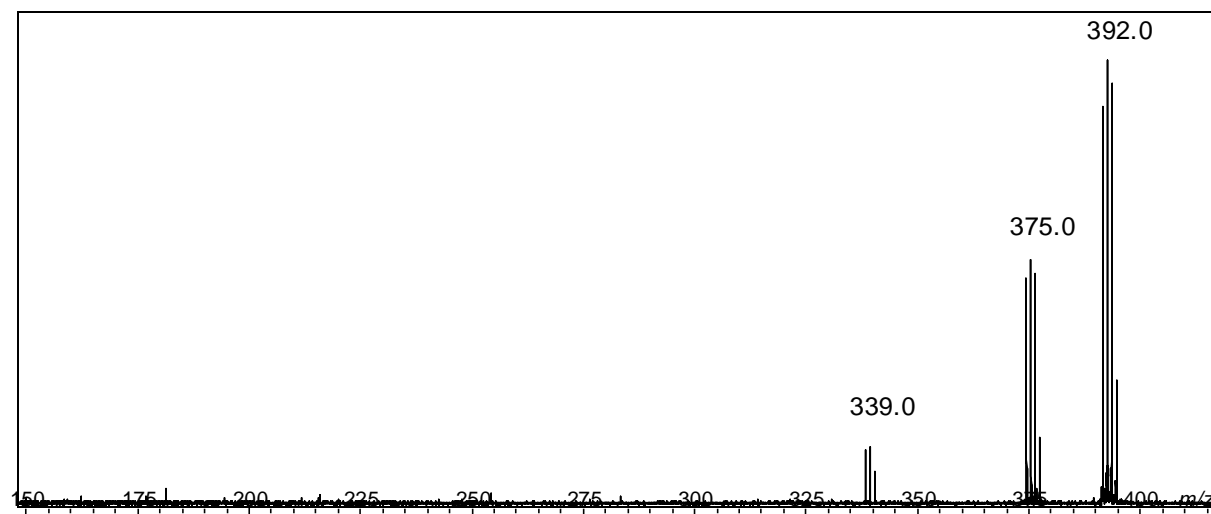


Figure S9. Positive ESI mass spectrum recorded upon selection of *cis*-[PtCl(NH₃)₂(4SU)]⁺ ion (m/z 391-395), in a hybrid FT-ICR tandem mass spectrometer (APEX-Qe Bruker Daltonics) after irradiation with CLIO FEL light on resonance at 1280 cm⁻¹.

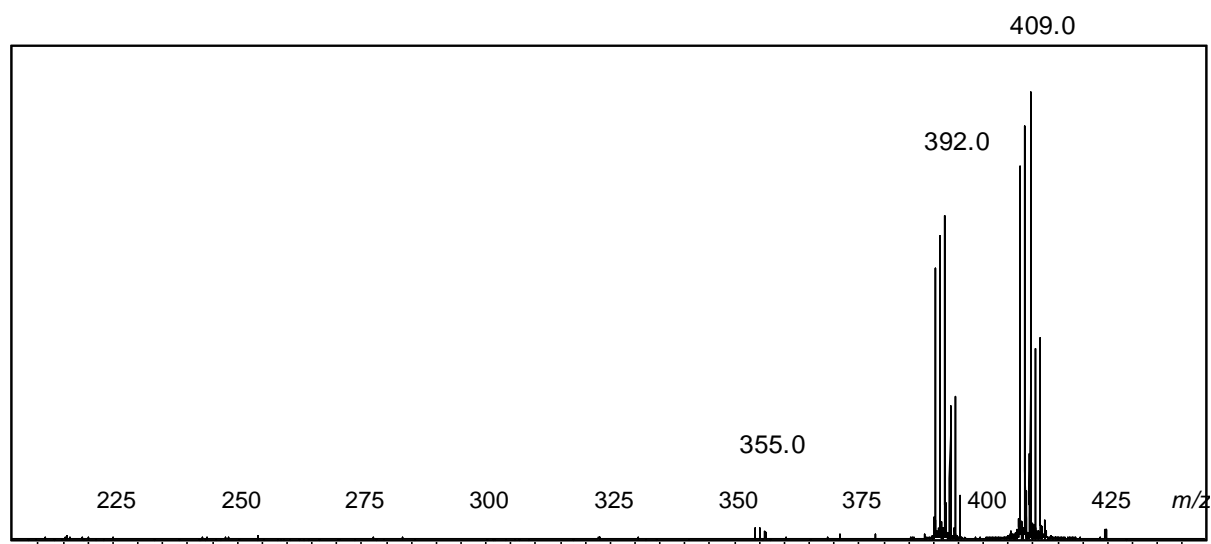


Figure S10. Positive ESI mass spectrum recorded upon selection of *cis*-[PtCl(NH₃)₂(24dSU)]⁺ ion (m/z 407-411), in a hybrid FT-ICR tandem mass spectrometer (APEX-Qe Bruker Daltonics) after irradiation with CLIO FEL light on resonance at 1285 cm⁻¹.

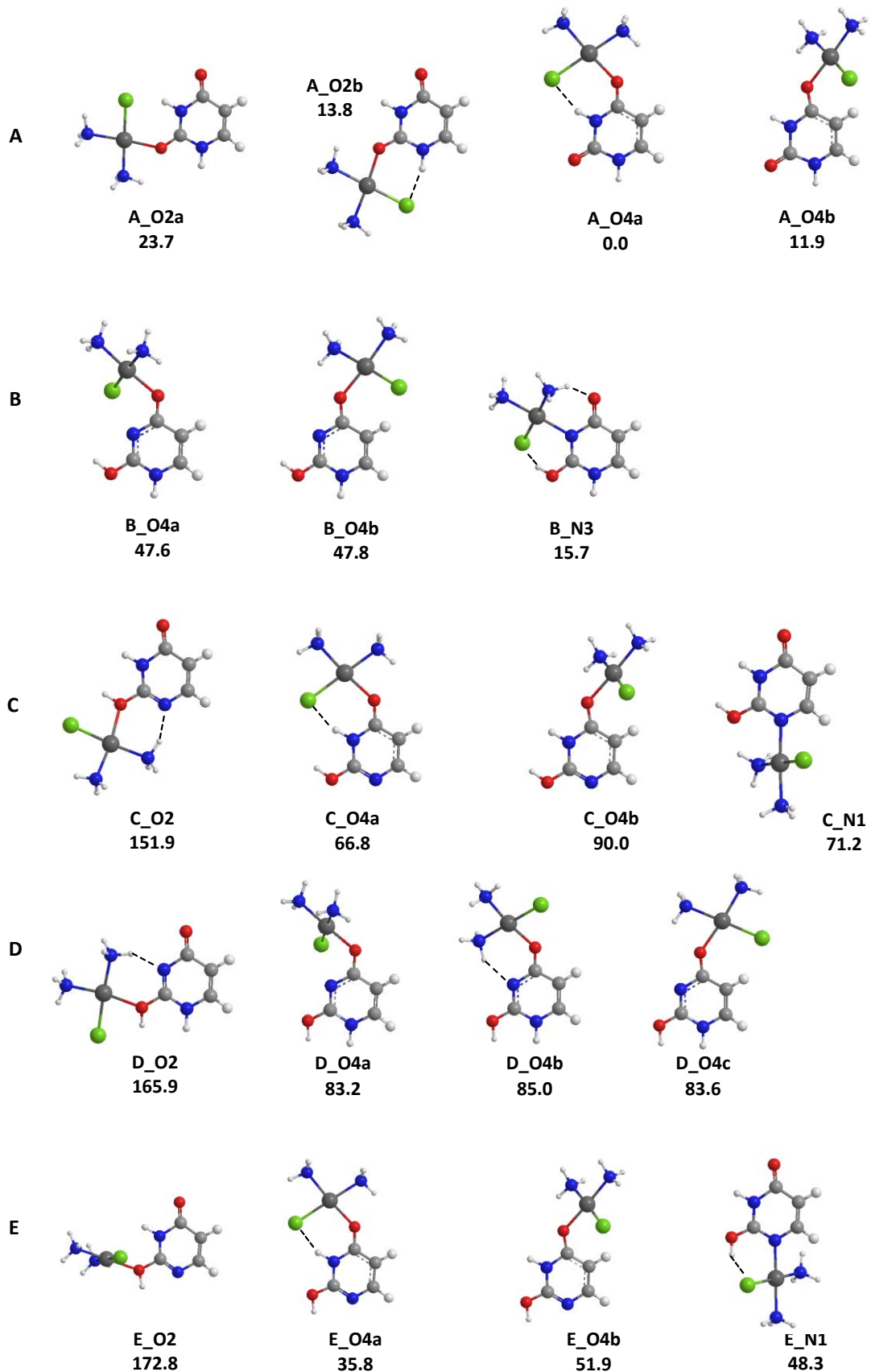


Figure S11a. Optimized geometries and relative free energy values (at the B3LYP/LACV3P/6-311G** level) at 298 K (kJ mol⁻¹) of *cis*-[PtCl(NH₃)₂(U)]⁺ conformer and isomer families A, B, C, D, E. Noncovalent interactions are marked by dashed lines. Distances are given in Å.

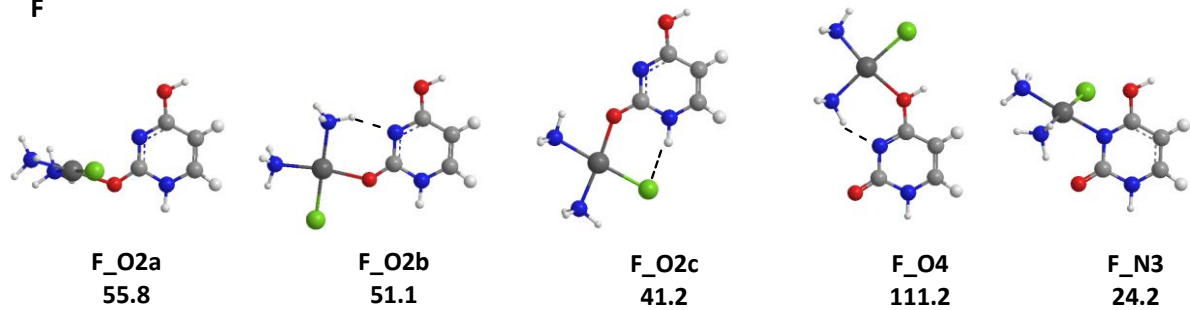
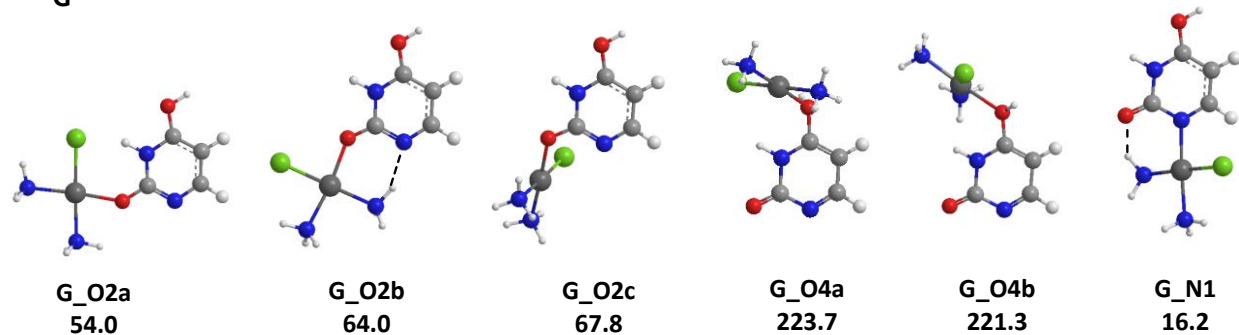
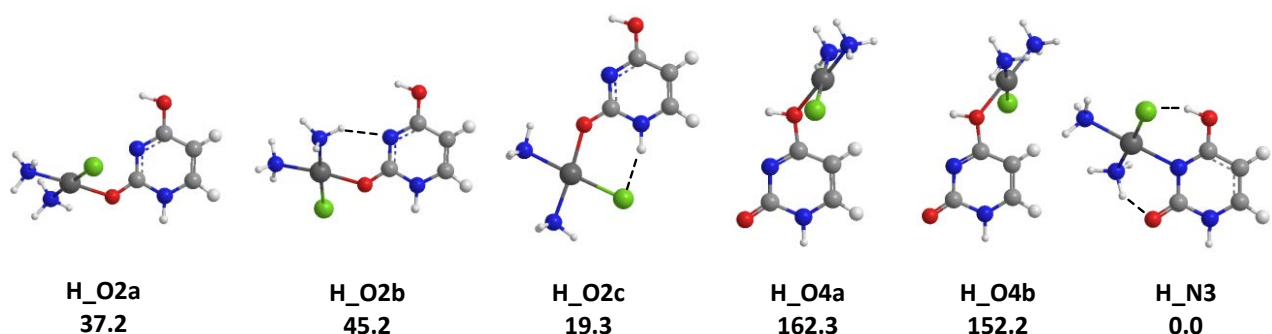
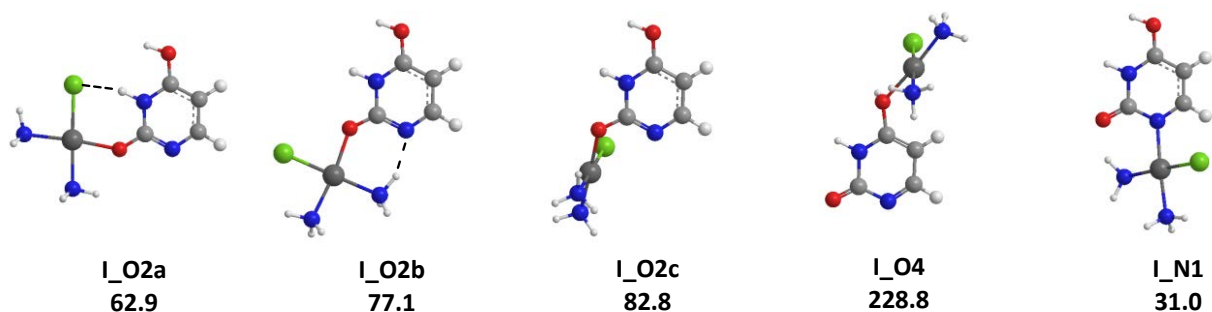
F**G****H****I**

Figure S11b. Optimized geometries and relative free energy values (at the B3LYP/LACV3P/6-311G** level) at 298 K (kJ mol⁻¹) of *cis*-[PtCl(NH₃)₂(U)]⁺ conformer and isomer families F, G, H, I. Noncovalent interactions are marked by dashed lines. Distances are given in Å.

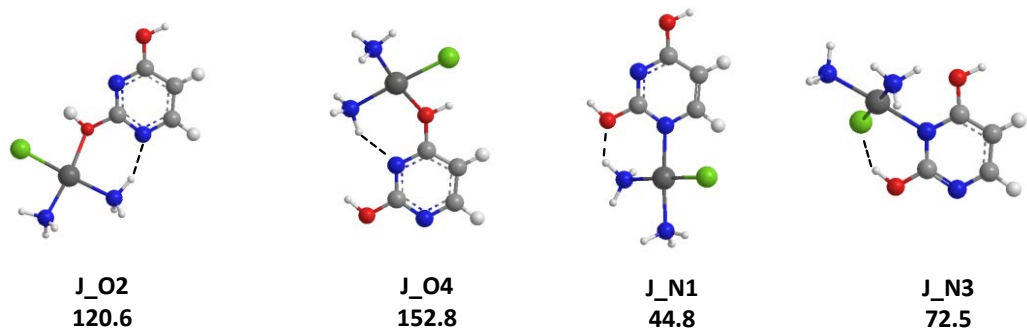
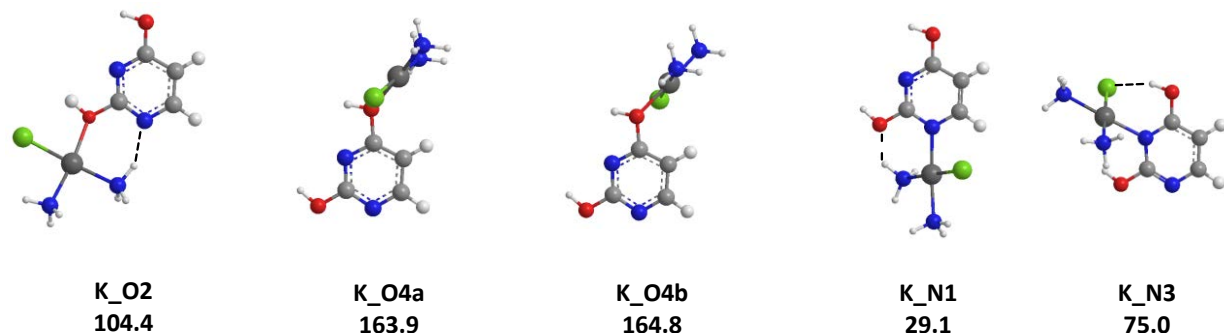
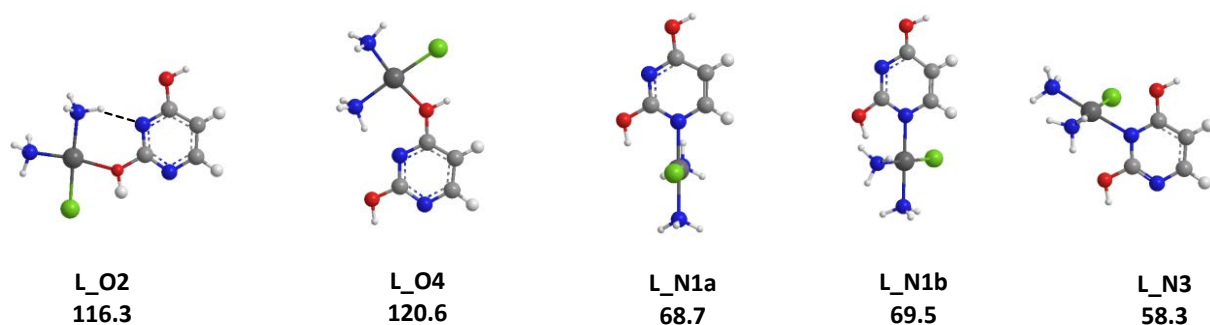
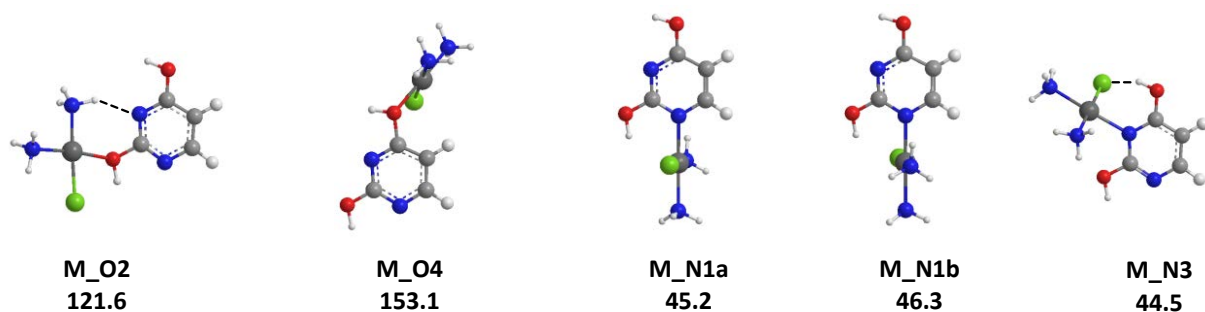
J**K****L****M**

Figure S11c. Optimized geometries and relative free energy values (at the B3LYP/LACV3P/6-311G** level) at 298 K (kJ mol⁻¹) of *cis*-[PtCl(NH₃)₂(U)]⁺ conformer and isomer families J, K, L, M. Noncovalent interactions are marked by dashed lines. Distances are given in Å.

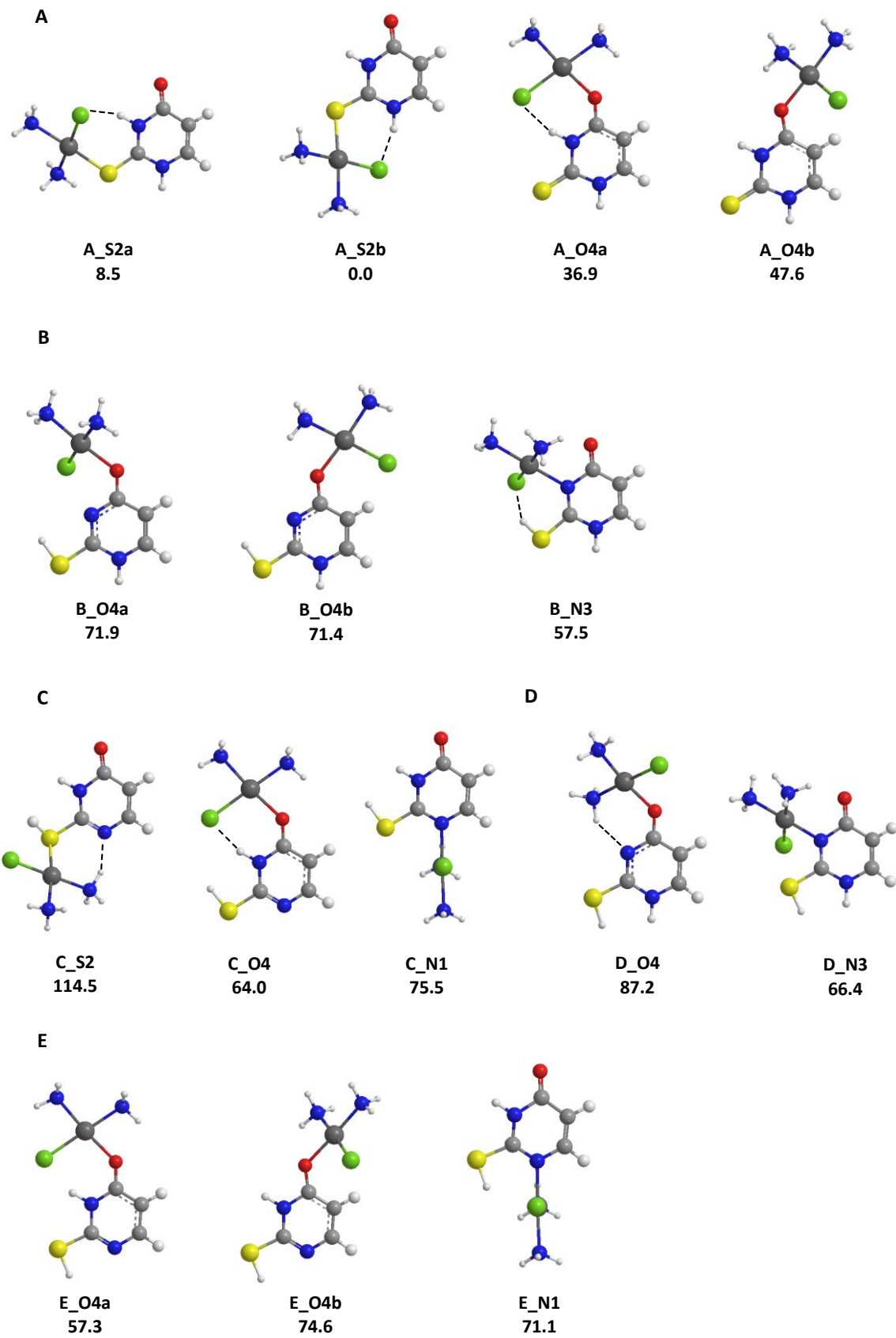


Figure S12a. Optimized geometries and relative free energy values (at the B3LYP/LACV3P/6-311G** level) at 298 K (kJ mol^{-1}) of *cis*- $[\text{PtCl}(\text{NH}_3)_2(2\text{SU})]^+$ conformer and isomer families A, B, C, D, E. Noncovalent interactions are marked by dashed lines. Distances are given in Å.

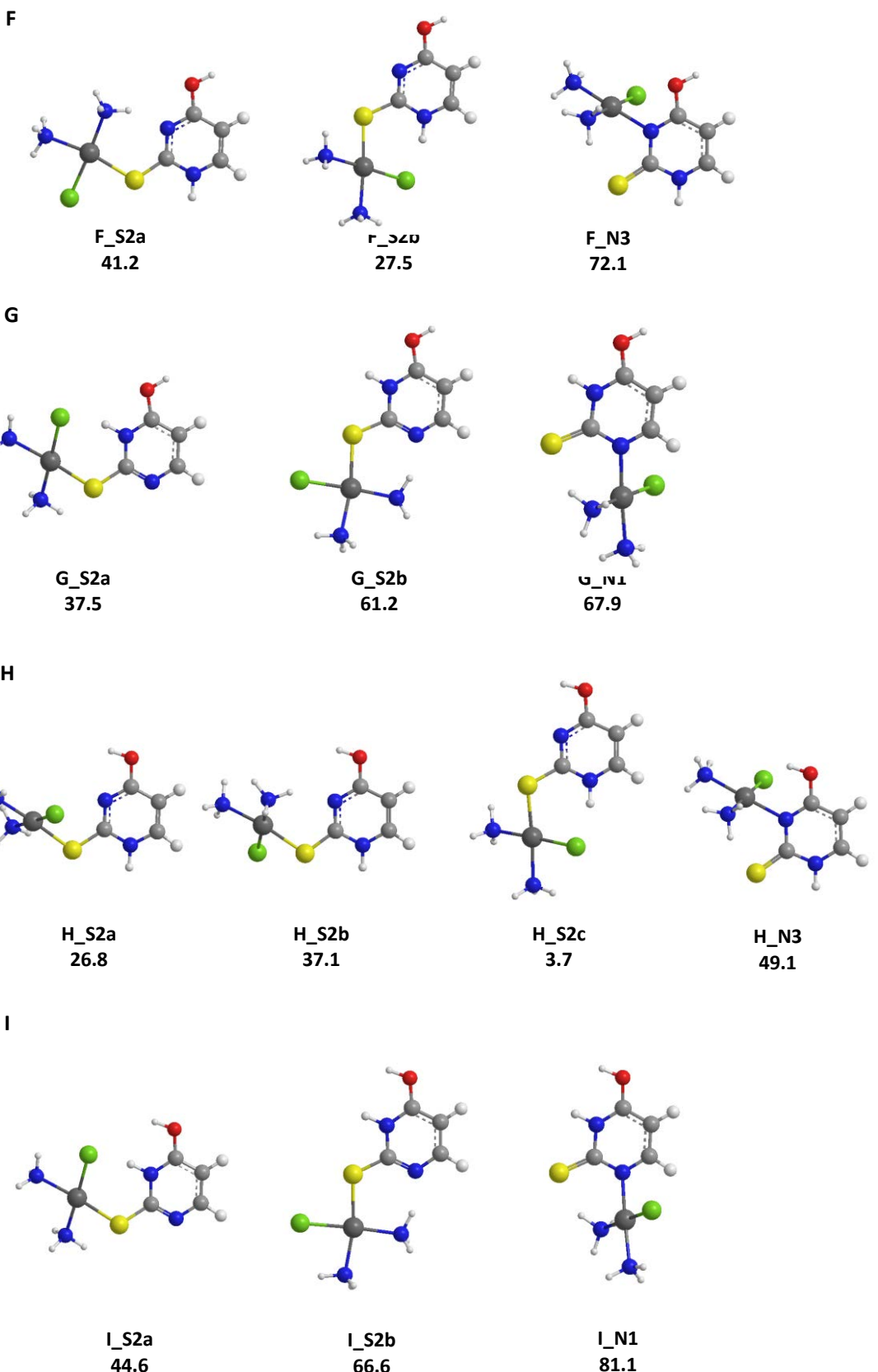


Figure S12b. Optimized geometries and relative free energy values (at the B3LYP/LACV3P/6-311G** level) at 298 K (kJ mol⁻¹) of *cis*-[PtCl(NH₃)₂(2SU)]⁺ conformer and isomer families F, G, H, I. Noncovalent interactions are marked by dashed lines. Distances are given in Å.

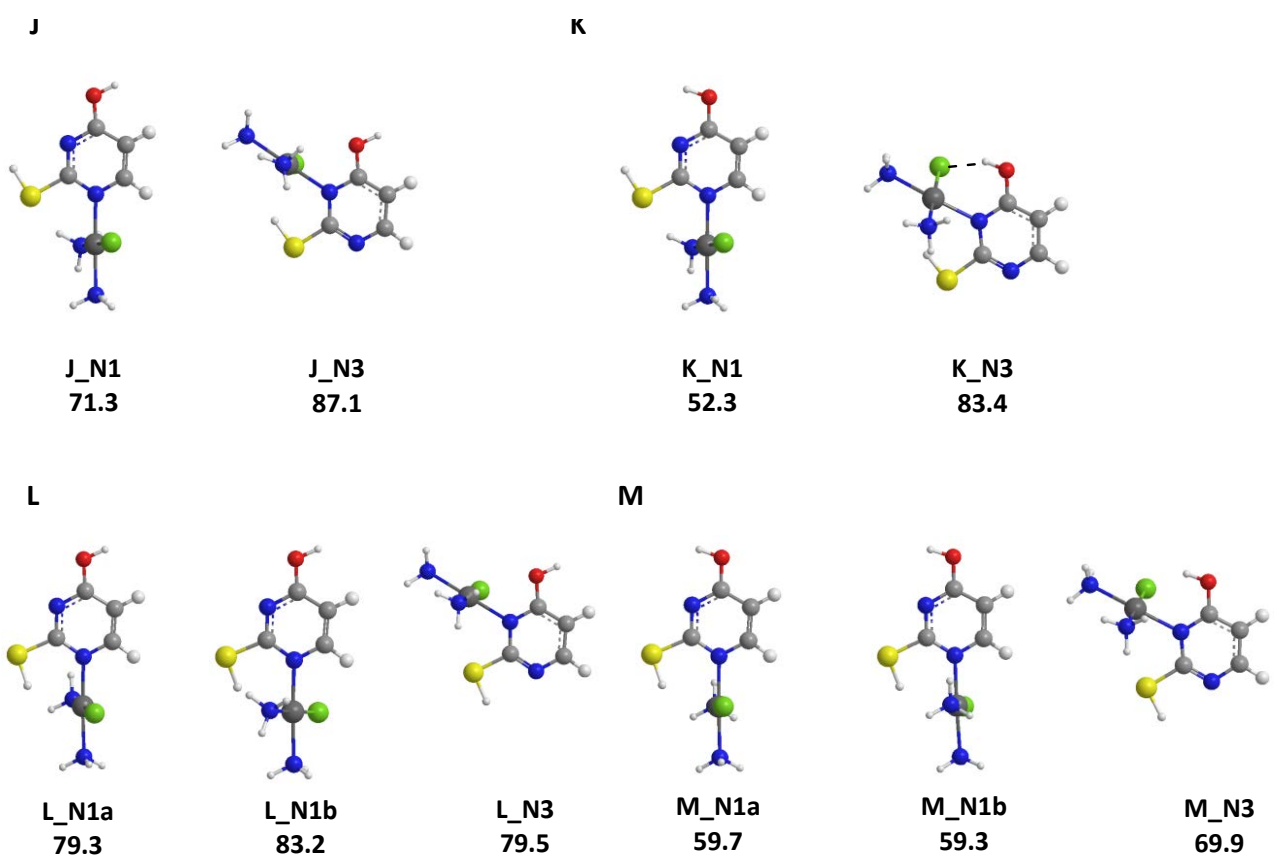


Figure S12c. Optimized geometries and relative free energy values (at the B3LYP/LACV3P/6-311G** level) at 298 K (kJ mol⁻¹) of *cis*-[PtCl(NH₃)₂(2SU)]⁺ conformer and isomer families J, K, L, M. Noncovalent interactions are marked by dashed lines. Distances are given in Å.

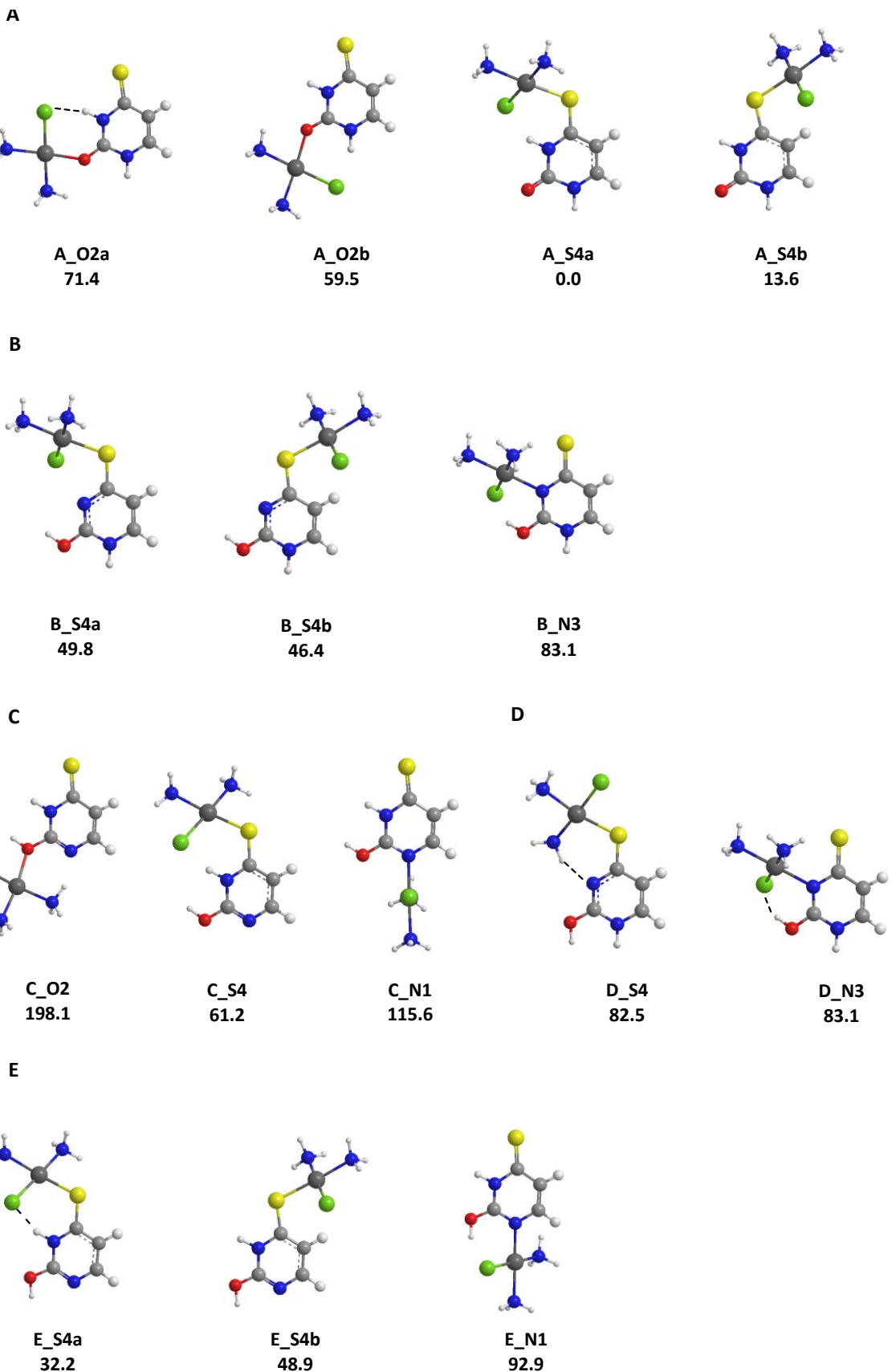


Figure S13a. Optimized geometries and relative free energy values (at the B3LYP/LACV3P/6-311G** level) at 298 K (kJ mol⁻¹) of *cis*-[PtCl(NH₃)₂(4SU)]⁺ conformer and isomer families A, B, C, D, E. Noncovalent interactions are marked by dashed lines. Distances are given in Å.

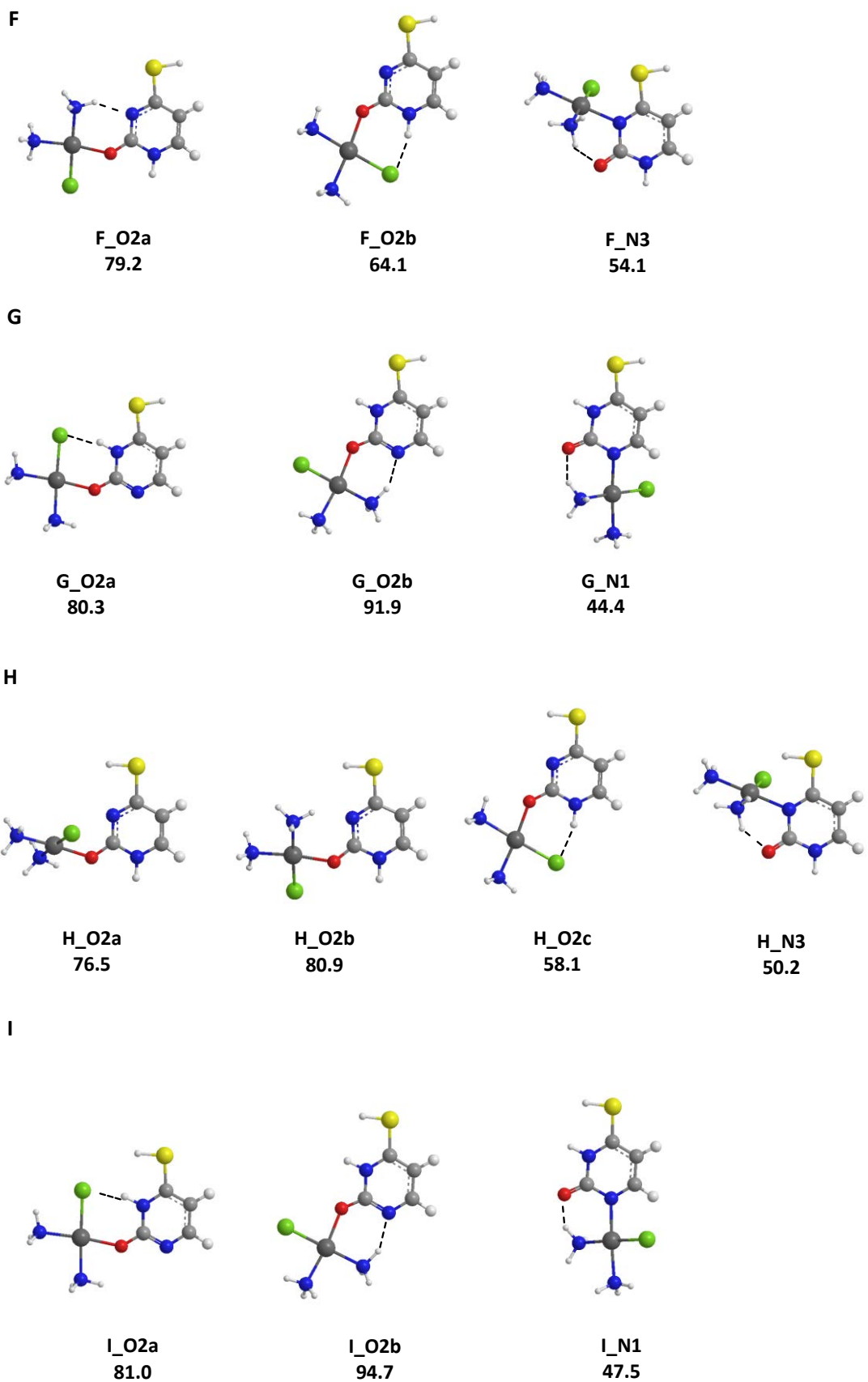


Figure S13b. Optimized geometries and relative free energy values (at the B3LYP/LACV3P/6-311G** level) at 298 K (kJ mol^{-1}) of *cis*- $[\text{PtCl}(\text{NH}_3)_2(4\text{SU})]^+$ conformer and isomer families F, G, H, I. Noncovalent interactions are marked by dashed lines. Distances are given in Å.

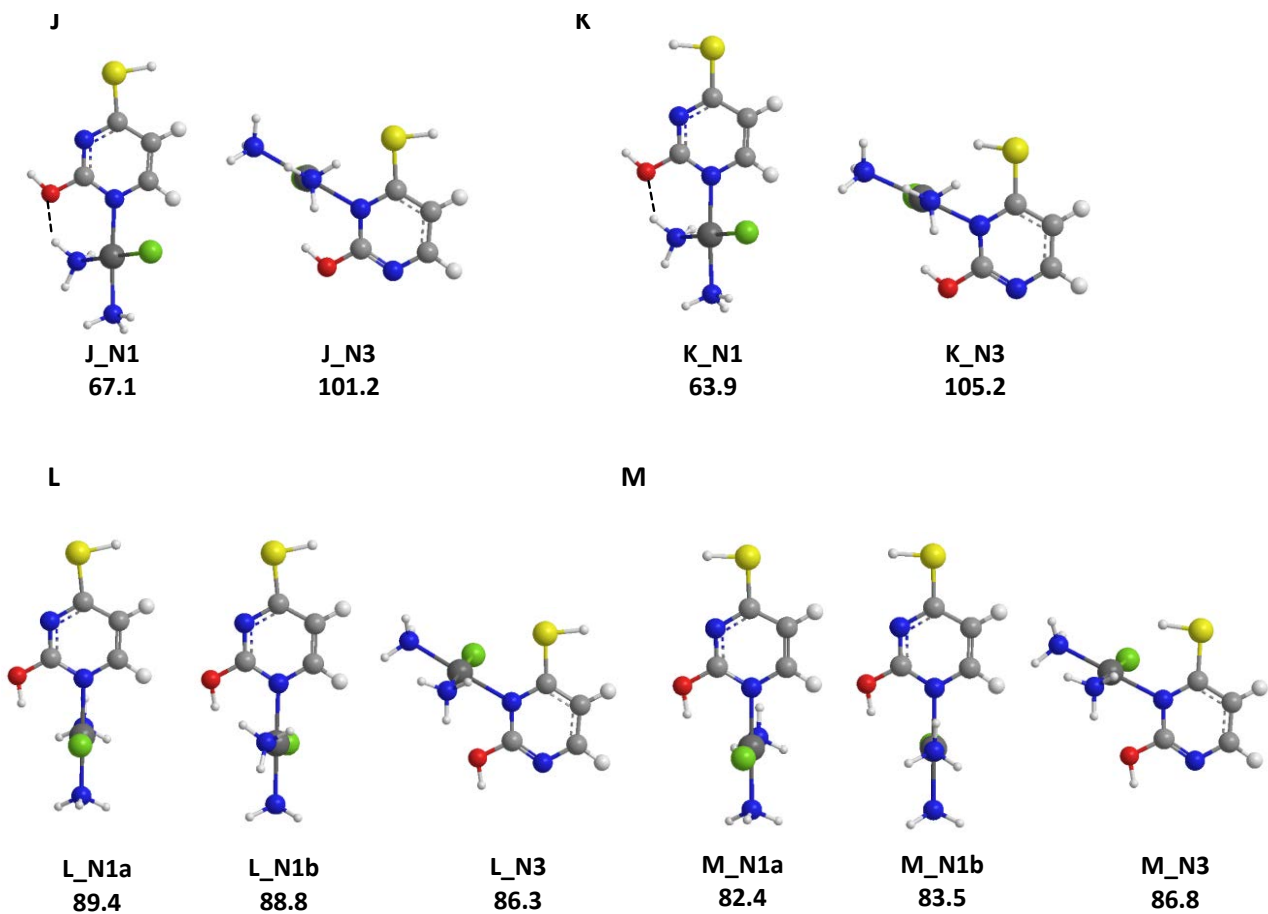


Figure S13c. Optimized geometries and relative free energy values (at the B3LYP/LACV3P/6-311G** level) at 298 K (kJ mol⁻¹) of *cis*-[PtCl(NH₃)₂(4SU)]⁺ conformer and isomer families J, K, L, M. Noncovalent interactions are marked by dashed lines. Distances are given in Å.

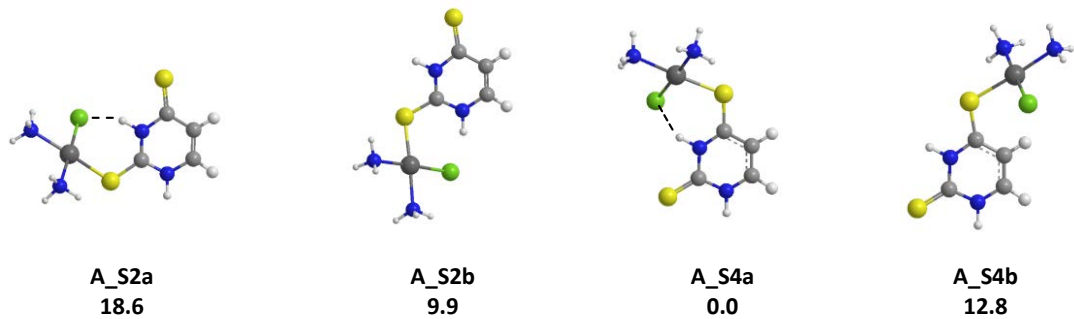
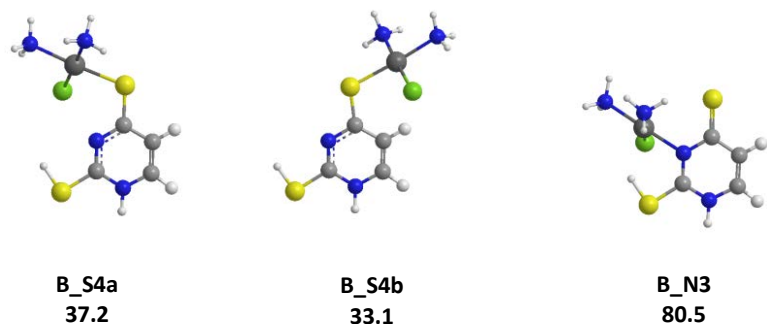
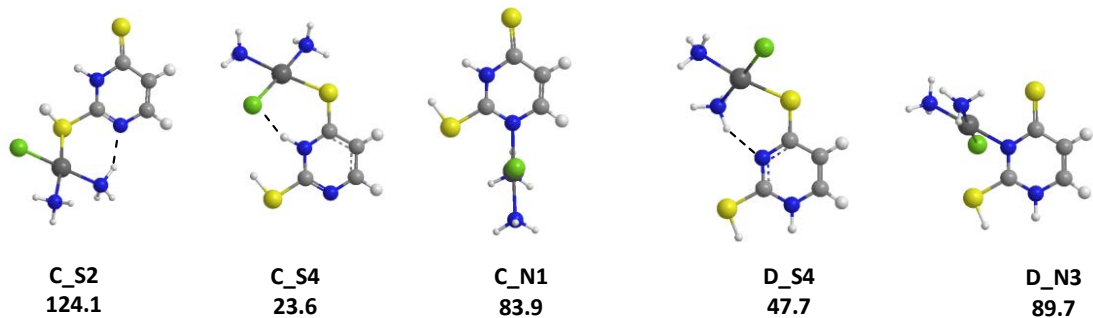
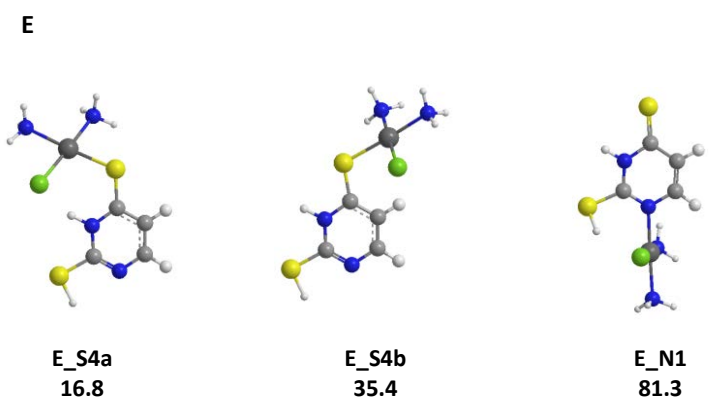
A**B****C****D**

Figure S14a. Optimized geometries and relative free energy values (at the B3LYP/LACV3P/6-311G** level) at 298 K (kJ mol⁻¹) of *cis*-[PtCl(NH₃)₂(24dSU)]⁺ conformer and isomer families A, B, C, D, E. Noncovalent interactions are marked by dashed lines. Distances are given in Å.

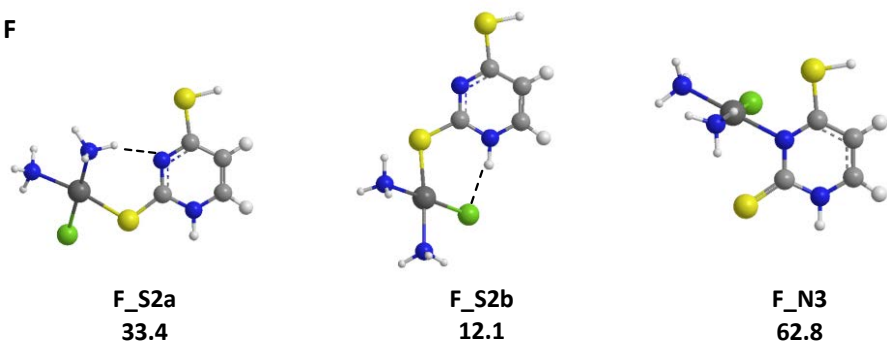
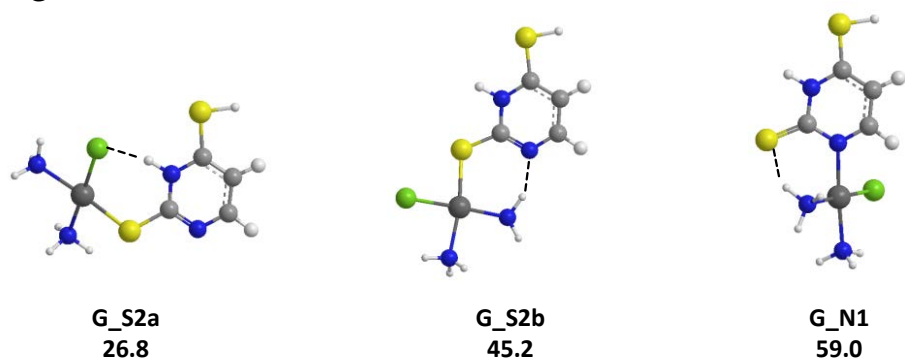
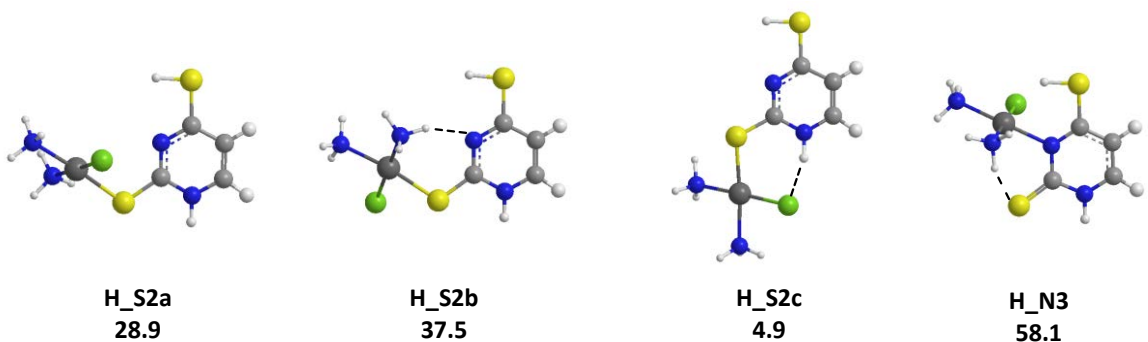
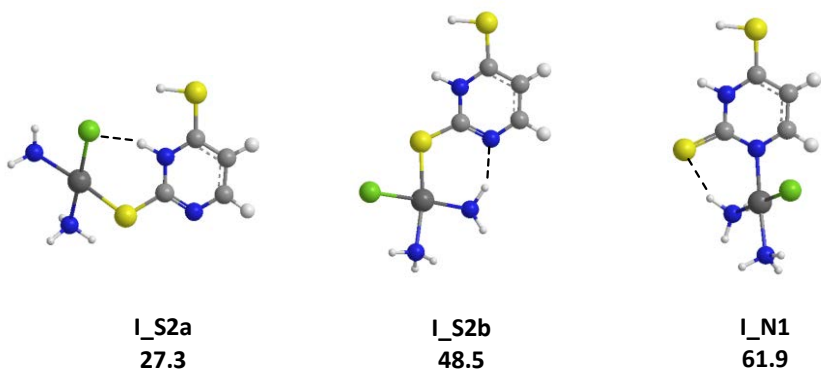
F**G****H****I**

Figure S14b. Optimized geometries and relative free energy values (at the B3LYP/LACV3P/6-311G** level) at 298 K (kJ mol⁻¹) of *cis*-[PtCl(NH₃)₂(24dSU)]⁺ conformer and isomer families F, G, H, I. Noncovalent interactions are marked by dashed lines. Distances are given in Å.

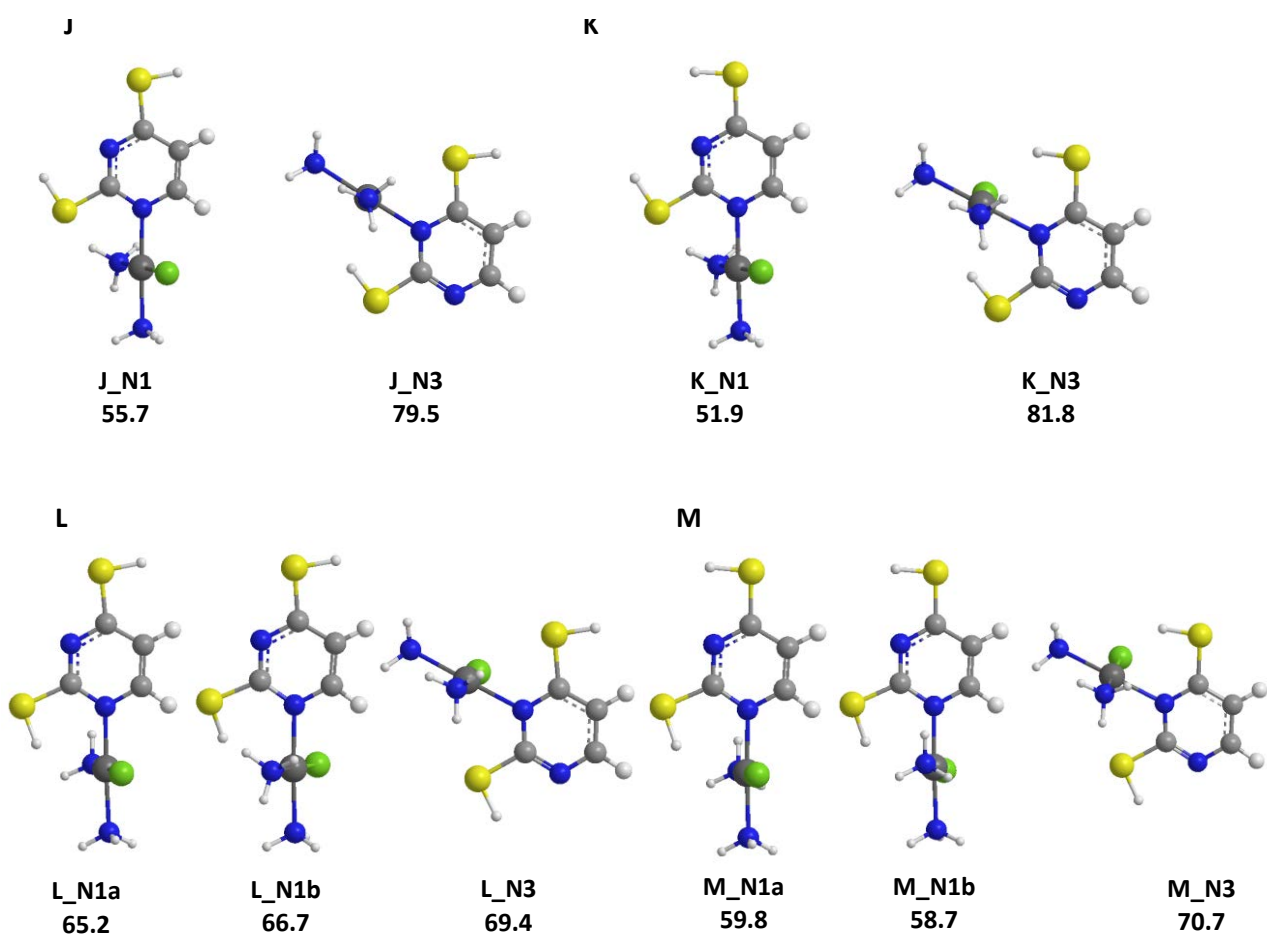


Figure S14c. Optimized geometries and relative free energy values (at the B3LYP/LACV3P/6-311G** level) at 298 K (kJ mol⁻¹) of *cis*-[PtCl(NH₃)₂(24dSU)]⁺ conformer and isomer families J, K, L, M. Noncovalent interactions are marked by dashed lines. Distances are given in Å.

Table S1. Thermodynamic data for conformers and isomers of *cis*-[PtCl(NH₃)₂(U)]⁺ calculated at the B3LYP/LACV3P/6-311G** level of theory.

Complex	ΔH° ₂₉₈ (kJ/mol)	ΔG° ₂₉₈ (kJ/mol)
A_O2a	33.0	23.7
A_O2b	23.4	13.8
A_O4a	8.5	0.0
A_O4b	20.2	11.9
B_O4a	55.6	47.6
B_O4b	57.3	47.8
B_N3	15.9	15.7
C_O2	160.7	151.9
C_O4a	73.8	66.8
C_O4b	99.1	90.0
C_N1	79.2	71.2
D_O2	174.7	165.9
D_O4a	93.8	83.2
D_O4b	92.6	85.0
D_O4c	92.9	83.6
E_O2	184.1	172.8
E_O4a	42.4	35.8
E_O4b	59.2	51.9
E_N1	53.4	48.3
F_O2a	66.5	55.8
F_O2b	58.5	51.1
F_O2c	48.5	41.2
F_O4	118.7	111.2
F_N3	26.9	24.2
G_O2a	61.1	54.0
G_O2b	72.2	64.0
G_O2c	78.5	67.8
G_O4a	237.8	223.7
G_O4b	239.4	221.3
G_N1	18.5	16.2
H_O2a	45.7	37.2
H_O2b	52.9	45.2
H_O2c	27.3	19.3
H_O4a	160.1	162.3
H_O4b	162.3	152.2
H_N3	0.0	0.0
I_O2a	70.3	62.9

I_O2b	86.0	77.1	
I_O2c	95.0	82.8	
I_O4	242.9	228.8	
I_N1	33.9	31.0	
J_O2	127.3	120.6	
J_O4	160.7	152.8	
J_N1	48.7	44.8	
J_N3	77.7	72.5	
K_O2	110.9	104.4	
K_O4a	175.2	163.9	
K_O4b	175.1	164.8	
K_N1	33.0	29.1	
K_N3	77.9	75.0	
L_O2	124.0	116.3	
L_O4	130.5	120.6	
L_N1a	76.5	68.7	
L_N1b	77.4	69.5	
L_N3	62.6	58.3	
M_O2	129.0	121.6	
M_O4	164.9	153.1	
M_N1a	52.9	45.2	
M_N1b	53.0	46.3	
M_N3	46.7	44.5	

Table S2. Thermodynamic data for conformers and isomers of *cis*-[PtCl(NH₃)₂(L)]⁺ (L=2SU, 4SU and 24dSU) calculated at the B3LYP/LACV3P/6-311G** level of theory.

Complex	ΔH° ₂₉₈ (kJ/mol)	ΔG° ₂₉₈ (kJ/mol)
2SU		
A_S2a	7.2	8.5
A_S2b	0.0	0.0
A_O4a	34.3	36.9
A_O4b	44.04	47.6
B_O4a	70.5	71.9
B_O4b	71.9	71.4
B_N3	48.5	57.5
C_S2	109.9	114.5
C_O4	61.2	64.0
C_N1	74.2	75.5
D_O4	85.3	87.2
D_N3	59.9	66.4
E_O4a	54.1	57.3
E_O4b	72.5	74.6
E_N1	71.9	71.1
F_S2a	38.1	41.2
F_S2b	23.9	27.5
F_N3	63.7	72.1
G_S2a	35.9	37.5
G_S2b	49.2	61.2
G_N1	60.2	67.9
H_S2a	26.0	26.8
H_S2b	33.8	37.8
H_S2c	1.1	3.7
H_N3	40.3	49.1
I_S2a	42.8	44.6
I_S2b	66.4	66.6
I_N1	73.9	81.1
J_N1	67.0	71.3
J_N3	85.4	87.1
K_N1	48.6	52.3
K_N3	76.7	83.4
L_N1a	79.5	79.3
L_N1b	78.8	83.2
L_N3	75.6	79.5
M_N1a	57.8	59.7
M_N1b	57.7	59.3
M_N3	64.5	69.9

4SU		
A_O2a	71.4	71.4
A_O2b	60.0	59.5
A_S4a	0.0	0.0
A_S4b	14.9	13.6
B_S4a	50.5	49.8
B_S4b	47.8	46.4
B_N3	75.5	83.1
C_O2	198.0	198.1
C_S4	61.3	61.2
C_N1	116.7	115.6
D_S4	81.1	82.5
D_N3	75.6	83.1
E_S4a	31.4	32.2
E_S4b	49.8	48.9
E_N1	88.7	92.9
F_O2a	79.3	79.2
F_O2b	62.9	64.1
F_N3	48.4	54.1
G_O2a	80.1	80.3
G_O2b	92.6	91.9
G_N1	39.2	44.4
H_O2a	77.3	76.5
H_O2b	81.8	80.9
H_O2c	58.4	58.1
H_N3	43.7	50.2
I_O2a	81.2	81.0
I_O2b	95.8	94.7
I_N1	43.2	47.5
J_N1	62.9	67.1
J_N3	100.3	101.2
K_N1	60.0	63.9
K_N3	104.9	105.2
L_N1a	89.3	89.4
L_N1b	90.4	88.9
L_N3	82.7	86.3
M_N1a	82.7	82.4
M_N1b	82.9	83.5
M_N3	82.4	86.8
24dSU		
A_S2a	20.2	18.6
A_S2b	11.8	9.9

A_S4a	0.0	0.0
A_S4b	14..0	12.8
B_S4a	39.9	37.2
B_S4b	36.4	33.1
B_N3	74.8	80.5
C_S2	121.5	124.1
C_S4	24.4	23.6
C_N1	85.1	83.9
D_S4	48.8	47.7
D_N3	85.8	89.7
E_S4a	17.6	16.8
E_S4b	38.2	35.4
E_N1	82.7	81.3
F_S2a	33.8	33.4
F_S2b	11.9	12.1
F_N3	57.4	62.8
G_S2a	29.2	26.8
G_S2b	47.6	45.2
G_N1	55.4	59.0
H_S2a	32.1	28.9
H_S2b	37.1	37.5
H_S2c	6.1	4.9
H_N3	51.9	58.1
I_S2a	29.3	27.3
I_S2b	50.9	48.5
I_N1	58.5	61.9
J_N1	55.0	55.7
J_N3	79.6	79.5
K_N1	51.2	51.9
K_N3	82.6	81.8
L_N1a	66.8	65.2
L_N1b	66.1	66.7
L_N3	68.9	69.4
M_N1a	61.2	59.8
M_N1b	61.0	58.7
M_N3	61.0	70.7

Table S3. Experimental and computed IR vibrational bands for cis-[PtCl(NH₃)₂(U)]⁺.**U_A_O4a**

Wavenumbers		DFT-computed	Vibrational mode ^b
Exp.	Calc. ^a		
1209	1205	92	δ N1H + δ CH
1290	1288	131	δ NH ₃ ' umbrella
	1324	99	δ NH ₃ umbrella
	1386	118	δ N3H
1426	1424	73	δ N1H
1480	1513	118	ν C4C5 + ν N1C6 + δ N1H
1580	1585	226	ν C4O4
1615	1630	986	ν C5C6
	1634	59	δ NH of NH ₃ and NH ₃ '
1800	1817	600	ν C2O2
	3183	580	ν N3H
	3346	58	ν NH ₂ asym of NH ₃
	3373	74	ν NH ₂ asym of NH ₃ '
	3384	46	ν NH ₂ asym of NH ₃
	3394	55	ν NH ₂ asym of NH ₃ '
3450	3448	185	ν N1H

a) Scaled by a factor of 0.974 in the fingerprint region and 0.957 in the X-H stretch region

b) NH₃' is the NH₃ trans to Cl**U_A_O4b**

Wavenumbers		DFT-computed	Vibrational mode ^b
Exp.	Calc. ^a		
1209	1210	109	δ N1H + δ CH
1290	1289	119	δ NH ₃ ' umbrella
	1319	104	δ NH ₃ umbrella
	1367	68	δ CH
1426	1417	71	δ N1H + ν C4C5
1480	1504	210	δ N1H + ν N3C4
1580	1571	361	ν C4O4 + δ N3H
	1615	179	δ NH ₂ sciss. of NH ₃ '
1615	1624	720	ν C5C6
	1635	53	δ NH of NH ₃ and NH ₃ '
1800	1819	764	ν C2O2
	3345	61	ν NH ₂ asym of NH ₃

	3379	59	νNH_2 asym of NH_3'
	3386	40	νNH_2 asym of NH_3
	3392	55	νNH_2 asym of NH_3'
	3580	100	νN3H
3450	3446	188	νN1H

a) Scaled by a factor of 0.974 in the fingerprint region and 0.957 in the X-H stretch region

b) NH_3' is the NH_3 trans to Cl

U_A_O2b

Exp.	Wavenumbers Calc. ^a	DFT-computed	Vibrational mode ^b
	1167	76	$\delta \text{C5H} + \nu \text{N3C4}$
1209	1212	47	δCH
1290	1297	116	$\delta \text{NH}_3'$ umbrella
	1328	89	δNH_3 umbrella
	1348	48	δN3H
1426	-		
1480	1466	148	νN1C2
1580	-		
1615	-		
	1635	59	δNH of NH_3 and NH_3'
	1639	910	$\nu \text{C2O2} + \nu \text{C5C6}$
	1656	547	$\nu \text{C5C6} + \delta \text{N1H}$
1800	1786	500	νC4O4
	3209	764	νN1H
	3346	67	νNH_2 asym of NH_3
	3373	71	νNH_2 asym of NH_3'
	3381	46	νNH_2 asym of NH_3
	3391	59	νNH_2 asym of NH_3'
3450	3435	78	νN3H

a) Scaled by a factor of 0.974 in the fingerprint region and 0.957 in the X-H stretch region

b) NH_3' is the NH_3 trans to Cl

Table S4: Experimental and computed IR vibrational bands for the *cis*-[PtCl(NH₃)₂(2SU)]⁺ complex

2SU_A_S2b

Wavenumbers		DFT-computed	Vibrational mode ^b
Exp.	Calc. ^a		
1145-1240	1170	170	δ C5H + ν N3C4 + ν C2S2
	1214	85	δ C6H
	1286	124	δ NH ₃ umbrella
1297	1305	117	δ NH _{3'} umbrella
1488	1463	80	ν N1C2
1560	1563	596	δ N1H
	1603	40	δ NH ₂ sciss. of NH ₃
1619	1637	53	δ NH of both NH ₃
	1643	40	ν C5C6
	1770	608	ν C4O4
	3154	689	ν N1H
	3362	49	ν NH ₂ asym of NH ₃
	3367	68	ν NH ₂ asym of NH _{3'}
	3387	37	ν NH ₂ asym of NH _{3'}
	3395	54	ν NH ₂ asym of NH ₃
3405	3409	86	ν N3H
3569	-		

a) Scaled by a factor of 0.974 in the fingerprint region and 0.957 in the X-H stretch region

b) NH_{3'} is the NH₃ trans to Cl

2SU_A_S2a

Wavenumbers		DFT-computed	Vibrational mode ^b
Exp.	Calc. ^a		
1145-1240	1178	195	δ C5H + ν N3C4 + ν C2S2
	1204	87	δ C6H
1297	1285	126	δ NH ₃ umbrella
	1298	112	δ NH _{3'} umbrella
1488	1465	175	ν N1C2
1560	1554	540	δ N1H + δ N3H
1619	1603	37	δ NH ₂ sciss. of NH ₃
	1618	28	δ NH ₂ sciss. of NH _{3'}
	1637	53	δ NH of NH ₃
	1641	47	ν C5C6
1770	1790	437	ν C4O4

	3242	314	ν N3H
	3286	34	ν NH ₃ sym
	3359	54	ν NH ₂ asym of NH ₃
	3372	69	ν NH ₂ asym of NH _{3'}
	3388	36	ν NH ₂ asym of NH _{3'}
3405	3396	53	ν NH ₂ asym of NH ₃
	3452	127	ν N1H
3569	-		

a) Scaled by a factor of 0.974 in the fingerprint region and 0.957 in the X-H stretch region

b) NH_{3'} is the NH₃ *trans* to Cl

2SU_H_S2c

Wavenumbers		DFT-computed	Vibrational mode ^b
Exp.	Calc. ^a		
1145-1240	1136	398	δ O4H
	1253	72	ν N1C2 + δ O4H
1297	1279	114	δ NH ₃ umbrella
	1297	143	δ NH _{3'} umbrella
1329	1329	83	ν N3C2 + δ CH
	1460	329	ν N3C4 + ν C4O4
1488	1515	240	δ N1H + ν C4C5
1560	1584	634	δ N1H+ ν N3C4
1619	1617	33	δ NH ₂ sciss. of NH ₃ and NH _{3'}
	1626	215	ν C5C6
1770	1628	42	δ NH ₂ twist. of NH ₃ and NH _{3'}
	1636	52	δ NH of NH ₃ and NH _{3'}
3405	3106	587	ν N1H
	3364	55	ν NH ₂ asym of NH _{3'}
	3366	62	ν NH ₂ asym of NH ₃
	3390	36	ν NH ₂ asym of NH _{3'}
3405	3397	49	ν NH ₂ asym of NH ₃
3569	3578	155	ν OH

a) Scaled by a factor of 0.974 in the fingerprint region and 0.957 in the X-H stretch region

b) NH_{3'} is the NH₃ *trans* to Cl

Table S5: Experimental and computed IR vibrational bands for the *cis*-[PtCl(NH₃)₂(4SU)]⁺ complex.

4SU_A_S4a

Wavenumbers		DFT-computed	Vibrational mode ^b
Exp.	Calc. ^a		
1098	1084	131	ν C4S4 + ν N1C2
1193	1170	144	ν C2N3
1279	1283	129	δ NH ₃ umbrella
	1298	120	δ NH _{3'} umbrella
	1413	84	δ N1H
1483	1500	56	δ N3H
	1512	84	δ N1H + δ N3H + ν C2O2
1609	1603	463	ν C5C6
	1604	162	δ NH ₂ sciss. of NH ₃
	1619	57	δ NH ₂ sciss. of NH _{3'}
	1638	48	δ NH of NH ₃ and of NH _{3'}
1808	1817	650	ν C2O2
	3222	330	ν N3H
	3361	54	ν NH ₂ asym of NH ₃
	3372	63	ν NH ₂ asym of NH _{3'}
	3390	36	ν NH ₂ asym of NH _{3'}
	3397	49	ν NH ₂ asym of NH ₃
3452	3441	230	ν N1H

a) Scaled by a factor of 0.974 in the fingerprint region and 0.957 in the X-H stretch region

b) NH_{3'} is the NH₃ trans to Cl

4SU_A_S4b

Wavenumbers		DFT-computed	Vibrational mode ^b
Exp.	Calc. ^a		
1098	1093	113	ν C4S4 + δ C5H
	1094	102	ring breathing
1193	-		
1279	1279	130	δ NH ₃ umbrella
	1296	119	δ NH _{3'} umbrella
	1408	78	δ N1H + ν N3C4
1483	1477	167	δ N3H
	1509	71	δ N1H + ν C6N1
1609	1597	593	ν C5C6
	1602	36	δ NH ₂ sciss. of NH ₃

	1619	46	$\delta \text{ NH}_2$ sciss. of NH_3'
	1649	49	$\delta \text{ NH}$ of NH_3 and of NH_3'
1808	1820	914	$\nu \text{ C}2\text{O}2$
	3360	57	$\nu \text{ NH}_2$ asym of NH_3
	3376	69	$\nu \text{ NH}_2$ asym of NH_3'
	3391	35	$\nu \text{ NH}_2$ asym of NH_3'
	3399	48	$\nu \text{ NH}_2$ asym of NH_3
	3406	93	$\nu \text{ N}3\text{H}$
3452	3440	235	$\nu \text{ N}1\text{H}$

a) Scaled by a factor of 0.974 in the fingerprint region and 0.957 in the X-H stretch region

b) NH_3' is the NH_3 *trans* to Cl

Table S6: Experimental and computed IR vibrational bands for the *cis*-[PtCl(NH₃)₂(24dSU)]⁺ complex.

24dSU_A_S4a

Wavenumbers		DFT-computed	Vibrational mode ^b
Exp.	Calc. ^a		
1094	1078	149	ν C4S4
	1095	154	ring breathing
1123	-		
1163	-		
1194	1184	197	ν N2C3
	1208	60	δ CH + ring breathing
1280	1283	134	δ NH ₃ umbrella
	1297	123	δ NH ₃ ' umbrella
1445	-		
	1496	73	δ N3H
1554	1556	618	δ N1H + δ N3H + ν C2S2
1586	1591	641	ν C5C6
	1619	42	δ NH ₂ sciss. of NH ₃ '
	1637	51	δ NH ₂ sciss. of NH ₃
	3224	304	ν N3H
3285	3271	27	ν NH ₃ sym.
	3290	16	ν NH ₃ ' sym.
3380	3361	55	ν NH ₂ asym of NH ₃
	3373	64	ν NH ₂ asym of NH ₃ '
	3390	35	ν NH ₂ asym of NH ₃ '
	3397	50	ν NH ₂ asym of NH ₃
3431	3434	189	ν N1H
3452	-		

a) Scaled by a factor of 0.974 in the fingerprint region and 0.957 in the X-H stretch region

b) NH₃' is the NH₃ *trans* to Cl

24dSU_A_S4b

Wavenumbers		DFT-computed	Vibrational mode ^b
Exp.	Calc. ^a		
1094	1076	173	δ N3H + ν C4S4
	1096	316	ring breathing
1123	-		
1163	-		
1194	1185	161	ν N2C3

	1208	47	ring breathing
1280	1279	128	$\delta \text{ NH}_3$ umbrella
	1292	124	$\delta \text{ NH}_3'$ umbrella
1445	-		
	1491	130	$\delta \text{ N3H}$
1554	1550	961	$\delta \text{ N1H} + \delta \text{ N3H} + \nu \text{ C2S2}$
1586	1585	624	$\nu \text{ C5C6}$
	1602	36	$\delta \text{ NH}_2$ sciss. of NH_3
	1619	41	$\delta \text{ NH}_2$ sciss. of NH_3'
	1638	46	$\delta \text{ NH}$ of NH_3 and of NH_3'
3285	3266	25	$\nu \text{ NH}_3$ sym
	3293	15	$\nu \text{ NH}_2$ asym of NH_3
3380	3376	63	$\nu \text{ NH}_2$ asym of NH_3'
	3391	35	$\nu \text{ NH}_2$ asym of NH_3'
	3398	48	$\nu \text{ NH}_2$ asym of NH_3
	3399	70	$\nu \text{ N3H}$
3431	3434	189	$\nu \text{ N1H}$
3452	-		

a) Scaled by a factor of 0.974 in the fingerprint region and 0.957 in the X-H stretch region

b) NH_3' is the NH_3 *trans* to Cl

Complete reference for Gaussian 09

Gaussian 09, Revision D.01, M. J. Frisch, G. W. Trucks, H. B. Schlegel, G. E. Scuseria, M. A. Robb, J. R. Cheeseman, G. Scalmani, V. Barone, B. Mennucci, G. A. Petersson, H. Nakatsuji, M. Caricato, X. Li, H. P. Hratchian, A. F. Izmaylov, J. Bloino, G. Zheng, J. L. Sonnenberg, M. Hada, M. Ehara, K. Toyota, R. Fukuda, J. Hasegawa, M. Ishida, T. Nakajima, Y. Honda, O. Kitao, H. Nakai, T. Vreven, J. A. Montgomery, Jr., J. E. Peralta, F. Ogliaro, M. Bearpark, J. J. Heyd, E. Brothers, K. N. Kudin, V. N. Staroverov, R. Kobayashi, J. Normand, K. Raghavachari, A. Rendell, J. C. Burant, S. S. Iyengar, J. Tomasi, M. Cossi, N. Rega, J. M. Millam, M. Klene, J. E. Knox, J. B. Cross, V. Bakken, C. Adamo, J. Jaramillo, R. Gomperts, R. E. Stratmann, O. Yazyev, A. J. Austin, R. Cammi, C. Pomelli, J. W. Ochterski, R. L. Martin, K. Morokuma, V. G. Zakrzewski, G. A. Voth, P. Salvador, J. J. Dannenberg, S. Dapprich, A. D. Daniels, Ö. Farkas, J. B. Foresman, J. V. Ortiz, J. Cioslowski, and D. J. Fox, Gaussian, Inc., Wallingford CT, 2009.